Thermodynamic properties in the evolution from BCS to Bose-Einstein condensation for a *d*-wave superconductor at low temperatures

R. D. Duncan and C. A. R. Sá de Melo
School of Physics, Georgia Institute of Technology, Atlanta, Georgia 30332
(Received 29 November 1999; revised manuscript received 26 May 2000)

The low-temperature evolution from BCS to Bose-Einstein condensation (BEC) for a two-dimensional *d*-wave superconductor is discussed at the saddle point (mean field) level. A systematic study of the changes of low-temperature thermodynamic properties is presented as a function of the charge carrier density and fixed interaction. It has been found that when the interaction strength is large enough, there is a critical density below which the single quasiparticle excitation spectrum develops a gap. At higher density of carriers and lower interaction strength (towards the BCS regime) the superconductor has gapless quasiparticle excitations, while at lower densities and higher interactions (towards the BEC regime) quasiparticle excitations are fully gapped. The appearance of a full gap in the quasiparticle excitation spectrum has dramatic consequences to the compressibility, specific heat, and spin susceptibility at low temperatures, as the critical density n_c is crossed. The change in behavior of these quantities indicates a possible quantum phase transition between a *d*-wave gapless phase and a *d*-wave fully gapped phase, as n_c is crossed.

I. INTRODUCTION

The problem of the evolution from BCS to BEC superconductivity is an old one[1–3] but recently it has received considerable attention in connection with high temperature superconductors.[4–13] Although high temperature superconductors are good candidates to test theories on the BCS to BEC evolution for *d*-wave superconductors, it must be emphasized that there is currently no experimental evidence that present a clear sign of this evolution as a function of particle density. However, the evolution from BCS to BEC superconductivity is by itself an interesting theoretical problem to study, specially for *d*-wave superconductors, as shall become clear in the next paragraph. As more experimental quantities are measured systematically as a function of density the applicability of the BCS to BEC evolution to high-temperature superconductors can be tested. Thus, in this work, we take the pragmatic approach of studying some experimentally measureable quantities at low temperatures as a function of density and we let experimentalists decide the applicability of these ideas when systematic studies are performed.

Very recently, initial theoretical studies of the BCS to Bose-Einstein evolution as a function of density were performed.[14–16] The nice works of den Hertog[15] and Andrenacci *et al.*[16] discussed the BCS to BEC evolution for a *d*-wave superconductor as a function of density in the lattice case, where an extended Hubbard model with attraction $(-|V|)$ between nearest-neighbor sites was used. In the work of den Hertog[15] a major rearrangement of the momentum distribution was found, when the chemical potential crossed the bottom of the electronic band, while Andrenacci *et al.*[16] observed a peculiar behavior in the pair size $\xi_{\rm pair}$ for a *d*-wave solution as a function of $|V|$ when the density approached half filling, and constructed nice phase diagrams of density versus interaction strength. The behavior of the momentum distribution and pair size for the *d*-wave case are quite different from the *s*-wave as emphasized in their work, but the evolution from BCS to BEC is still regarded as a crossover. In the continuum case, it was first noticed by Borkowski and Sá de Melo[14] that the appearance of a full gap in the BCS to BEC evolution for a *d*-wave superconductor lead to (a) a discontinuity in the momentum distribution when the chemical potential crossed zero, (b) dramatic changes in the density of states, and (c) qualitative changes in the specific heat and spin susceptibility. These results were argued to be evidence for a possible quantum phase transition separating a gapless *d*-wave superconductor from a fully gapped *d*-wave superconductor. A similar quantum phase transition should be present in the lattice case for a *d*-wave superconductor, however, this was not reported in the recent literature.[15,16]

In this paper, we extend the results of Borkowski and Sá de Melo[14] and address in detail the evolution from a BCS to a BEC *d*-wave superconductor at low temperatures, within the saddle point (mean field) approximation for a continuum model. Corrections due to collective modes are also briefly discussed. For this purpose we study single quasiparticle properties (excitation spectrum, and momentum distribution) and thermodynamic quantities (compressibility, spin susceptibility, and specific heat) as a function of particle density at fixed interaction strength. Based on our findings regarding the compressibility, spin susceptibility and specific heat, we argue that a quantum phase transition for a *d*-wave superconductor occurs when the chemical potential crosses zero for a fixed interaction strength and changing density.

Quite generally the evolution from BCS to BEC superconductivity can be characterized by two parameters: the chemical potential μ and the Cooper pair size $\xi_{\rm pair}$. The BCS limit is characterized by a positive chemical potential $\mu=\epsilon_F$ and a large size of Cooper pairs ($\xi_{\rm pair}\gg k_F^{-1}$), while the BEC regime is characterized by a large and negative chemical potential $\mu=-E_b^{(l)}/2$, where $E_b^{(l)}$ is the binding energy of the two-body problem in the lth angular momentum channel, and by a small size of pairs ($\xi_{\rm pair}\ll k_F^{-1}$). Here

$l=0$ (or s) indicates the s-wave channel, while $l=2$ (or d) indicates the d-wave channel. The excitation spectrum at zero temperature has the form $E_l(\mathbf{k})=[(\epsilon_{\mathbf{k}}-\mu)^2+|\Delta_l(\mathbf{k})|^2]^{1/2}$, where $\epsilon_{\mathbf{k}}=k^2/2m$ and $\Delta_l(\mathbf{k})=\Delta_{0l}h_l(k)\cos(l\phi)$, with $k=|\mathbf{k}|$.

In the s-wave case the excitation spectrum $E_s(\mathbf{k})$ is gapped for all $\mathbf{k}$, and it increases smoothly from the BCS to the BEC limit. As a result the quantities that depend directly on the excitation spectrum $E_s(\mathbf{k})$ also evolve smoothly. For instance, the quasiparticle density of states $N_s(\omega)$ at low frequencies is always zero, since there are no available states inside the gap. Thus, contributions from single quasiparticle excitations to thermodynamic quantities are always exponentially small at low temperatures. In the d-wave case the situation is qualitatively different. For $\mu>0$ the superconductor is gapless at the Dirac points $k=k_\mu=\sqrt{2m\mu}$, $\phi=\pm\pi/4$, $\pm 3\pi/4$, while for $\mu<0$ the superconductor acquires a finite gap. The line $\mu=0$ separates two regimes with qualitatively different behavior. This has important consequences for the momentum distribution, and density of states. The quasiparticle density of states $N_d(\omega)$ changes discontinuously at low frequencies from linear in ω for $\mu>0$ [where $E_d(\mathbf{k})$ is linear in momentum close to the Dirac points], to a constant at $\mu=0$ [where $E_d(\mathbf{k})$ is quadratic for small momenta], to zero for $\mu<0$ [where $E_d(\mathbf{k})\simeq|\mu|+\mathcal{O}(k^2)$ for small k]. Thus, contributions from single quasiparticle excitations to thermodynamic quantities at low temperatures also exhibit singular behavior in the vicinity of $\mu=0$. In particular, the zero temperature compressibility diverges when $\mu=0$ at a critical density n_c for fixed interaction, indicating the possibility of a quantum phase transition.

The rest of the paper is organized as follows. In Sec. II, we discuss the Hamiltonian and the ground state energy of the system. In Sec. III, we discuss the saddle point and number equations deduced from the ground state energy, while in Sec. IV the quasiparticle excitation spectrum is discussed and an interaction versus density phase diagram is constructed. In Sec. V, the momentum distribution is analyzed. Section VI contains a description of the compressibility of the system as the BCS to BEC evolution takes place. In Secs. VII and VIII, we discuss the opposite spin density-density correlations and the Cooper pair size, respectively. In Sec. IX topological considerations are presented. In Sec. X the low-temperature spin susceptibility and specific heat are analyzed within the BCS to BEC evolution. Finaly, Sec. XI contains the summary of our results.

II. HAMILTONIAN

In order to analyze the low-temperature thermodynamic properties from the BCS to BEC limit, we start with the two-dimensional Hamiltonian

$$H=\sum_{\mathbf{k}\sigma}(\epsilon_{\mathbf{k}}-\mu)\psi^\dagger_{\mathbf{k}\sigma}\psi_{\mathbf{k}\sigma}+\sum_{\mathbf{k}\mathbf{k}'\mathbf{q}}V_{\mathbf{k}\mathbf{k}'}b^\dagger_{\mathbf{k}\mathbf{q}}b_{\mathbf{k}'\mathbf{q}}, \tag{1}$$

where $b_{\mathbf{k}\mathbf{q}}=\psi_{-\mathbf{k}+\mathbf{q}/2\downarrow}\psi_{\mathbf{k}+\mathbf{q}/2\uparrow}$. The interaction potential $V_{\mathbf{k}\mathbf{k}'}$ is expanded in its angular momentum components as

$$V_{\mathbf{k}\mathbf{k}'}=\sum_{l=-\infty}^{+\infty}V^{(l)}_{kk'}\exp(il\phi_{\mathbf{k}\mathbf{k}'}), \tag{2}$$

where $\phi_{\mathbf{k}\mathbf{k}'}=\mathrm{acos}(\hat{\mathbf{k}}\cdot\hat{\mathbf{k}}')$ is the angle betwen the vectors $\mathbf{k}$ and $\mathbf{k}'$ and $V^{(l)}_{kk'}=2\pi\int_0^\infty dr r J_l(kr)J_l(k'r)V(r)$. The index l labels angular momentum states in two spatial dimensions, with $l=0,\pm1,\pm2,\ldots$, corresponding to $s,p,d,\ldots$, channels, respectively. A possible choice of the real space potential is

$$V(r)=V_1\Theta(R_1-r)+V_0\Theta(r-R_1)\Theta(R_0-r), \tag{3}$$

which is repulsive at short distances $r<R_1$, attractive at intermediate distances $R_1<r<R_0$, and vanishes for $r>R_0$. This class of potentials includes (a) the delta function potential with zero range ($V_1\to-\infty$, $V_0=0$, and $R_1=R_0=0$); (b) the attractive potential with range R_0 ($V_1<0$, $V_0=0$, and $R_1=R_0$); and (c) the short range repulsive, intermediate range attractive potential with range R_0 ($V_1>0$, $V_0<0$, and $R_1\neq R_0$). A d-wave type solution can be considered for the real space potential $V(r)$ in Eq. (3), when $V_1>0$ and $V_0<0$. This choice was made in a previous paper for the continuum case,[14] and corresponds in the lattice case to the choices $U>0$ and $V<0$ in the extended Hubbard model studied by Andrenacci *et al.*[16]

Under these circumstances, quite generally it is not possible to find a separable potential in momentum space $V_{\mathbf{k}\mathbf{k}'}=-\lambda w^*(\mathbf{k})w(\mathbf{k}')$, nevertheless in the spirit of Ref. 3 we choose to study a separable potential that contains most of the general features described above. We consider only singlet superconductivity, and since we do not discuss a mechanism for s-wave or d-wave superconductivity, the s-wave and the d-wave channels are studied separately. For this purpose, we use the separable potential

$$V_{\mathbf{k}\mathbf{k}'}=-\lambda_l w_l(\mathbf{k})w_l(\mathbf{k}'). \tag{4}$$

The interaction term $w_l(\mathbf{k})$ can be written as the product of two functions, $w_l(\mathbf{k})=h_l(k)g_l(\hat{\mathbf{k}})$, where $h_l(k)=(k/k_1)^l/[1+(k/k_0)]^{l+1/2}$ controls the range of the interaction and $g_l(\hat{\mathbf{k}})=\cos(l\phi)$ is the angular dependence of the interaction. Here $k_0\sim R_0^{-1}$, where R_0 plays the role of the interaction range, and k_1 sets the scale at low momenta. The momentum scales k_0 and k_1 are not momentum cutoffs, they merely set the momentum scales in the short wavelength limit (large momenta) (k_0), and the long wavelength limit (small momenta) (k_1). They are necessary to produce the physically correct behavior of $V^{(l)}_{k,k'}$ for the real space potential $V(r)$, i.e., this form of $w_l(\mathbf{k})$ generates the correct lth-channel behavior of $V^{(l)}_{k,k'}$ for both low and high momenta.[17]

Strictly at $T=0$ the choice of the variational wave function $|\Psi\rangle=\Pi_{\mathbf{k}}(u_{\mathbf{k}}+v_{\mathbf{k}}\psi^\dagger_{\mathbf{k},\uparrow}\psi^\dagger_{-\mathbf{k},\downarrow})|0\rangle$ leads to a good description of the BCS to BEC evolution[2] and coincides with the field theoretical description based on functional integration[12] of the ground state properties. Either one of these approaches lead to the ground state energy given by the expression

$$W_l=2\sum_{\mathbf{k}}(\epsilon_{\mathbf{k}}-\mu)v^2_{\mathbf{k}}+\sum_{\mathbf{k},\mathbf{k}'}V^{(l)}_{\mathbf{k},\mathbf{k}'}u_{\mathbf{k}}v_{\mathbf{k}}u_{\mathbf{k}'}v_{\mathbf{k}'}, \tag{5}$$

where $u^2_{\mathbf{k}}+v^2_{\mathbf{k}}=1$. At this stage we have considered only the part of the general interaction involving $(-\mathbf{k},\mathbf{k})$ electrons states, assumed that pairing occurs with the same total center of mass momentum $\mathbf{q}=0$, and neglected any residual

interactions.[18] This initial level of approximation corresponds to a saddle point description in the functional integral language[12] and will be described next.

III. SADDLE POINT AND NUMBER EQUATIONS

To find the saddle point and number equations we need to minimize the ground state energy W_l with respect to $v_{\mathbf{k}} = \sqrt{n_l(\mathbf{k})}$ and to fix the particle density $n = -\partial W_l/\partial\mu$. Using the separable potential of Eq. (4), this minimization process leads to the saddle point equation

$$\frac{1}{\lambda_l} = \sum_{\mathbf{k}} \frac{|w_l(\mathbf{k})|^2}{2E_l(\mathbf{k})}, \tag{6}$$

and to the number equation

$$n = 2\sum_{\mathbf{k}} n_l(\mathbf{k}), \tag{7}$$

where $n_l(\mathbf{k})$ is the momentum distribution given by

$$n_l(\mathbf{k}) = [1 - (\epsilon_{\mathbf{k}} - \mu)/E_l(\mathbf{k})t]/2, \tag{8}$$

$E_l(\mathbf{k})$ is the quasiparticle excitation energy given by

$$E_l(\mathbf{k}) = [(\epsilon_{\mathbf{k}} - \mu)^2 + |\Delta_l(\mathbf{k})|^2]^{1/2}, \tag{9}$$

and $\Delta_l(\mathbf{k}) = \Delta_{0l} w_l(\mathbf{k})$ is the order parameter. For a given interaction range $R_0 \sim k_0^{-1}$, the evolution from the BCS limit (largely overlaping pairs) to the BEC limit of (weakly overlapping pairs) may occur either by changing the attraction strength λ_l or the density n ($n = k_F^2/2\pi$). In either case, this evolution can be safely analyzed with the approximations used here provided that the system is *dilute* enough ($k_F^2 \ll k_0^2$),[19] i.e., the square of the interparticle spacing ($\sim k_F^{-1}$) is much larger than the square of the interaction range ($\sim k_0^{-1}$). This means that below a maximum density $n_{\max} \sim k_{F\max}^2$, the square of the interaction range R_0 is much smaller than the square of the interparticle spacing $k_{F_{\max}}^{-1}$, $R_0^2 \ll k_{F_{\max}}^{-2}$, or equivalently $(k_0/k_{F_{\max}})^2 \gg 1$. Thus, $k_{F_{\max}}$ is the largest value of k_F allowed that still satisfies the diluteness condition above. We choose to scale all energies with respect to the maximal Fermi energy $\epsilon_{F_{\max}} = k_{F_{\max}}^2/2m$, which fixes the maximum density $n = n_{\max} = 2\rho_{2D}\epsilon_{F_{\max}}$, and to scale all momenta with respect to $k_{F_{\max}} = \sqrt{2m\epsilon_{F_{\max}}}$. The coupling constant λ_l is scaled with respect to the two-dimensional density of states ρ_{2D}. From now on we use this scaling. The parameter $k_{F_{\max}}$ can be defined, for instance, as (a) $k_{F_{\max}} = k_0/10$ or (b) $k_{F_{\max}} = k_0/\sqrt{10}$, provided that $(k_0/k_{F_{\max}})^2 \gg 1$. If we choose $k_0 = 1$ Å^{-1} (an interaction range $R_0 \approx 1$ Å), then in case (a) $k_{F_{\max}} = 0.1$ Å^{-1} or $n_{\max} = 1.59\times 10^{13}$ cm^{-2}, and in case (b) $k_{F_{\max}} = 0.32$ Å^{-1} or $n_{\max} = 1.59\times 10^{14}$ cm^{-2}. Or if we choose $k_0 = 10$ Å^{-1} (an interaction range $R_0 \approx 0.1$ Å), then in case (a) $k_{F_{\max}} = 1$ Å^{-1} or $n_{\max} = 1.59\times 10^{15}$ cm^{-2}, and in case (b) $k_{F_{\max}} = 3.16$ Å^{-1} or $n_{\max} = 1.59\times 10^{16}$ cm^{-2}.

In these dimensionless units, the parameter $\zeta = \lambda_l/n$ characterizes the BCS to BEC evolution. The BCS limit is reached only when $\zeta \ll 1$ and the BEC limit is reached only when $\zeta \gg 1$. The numerical solutions for Δ_{0d} (*d*-wave case) and μ, when $k_1 = k_0 = 10$ are shown in Fig. 1, for fixed interaction strength $\lambda_d = 8.2$, and changing density n. We choose identical values of k_0 and k_1 for simplicity only. For $k_1 = k_0 = 10$ and for $\lambda_d < 8$ the chemical potential μ never changes sign as a function of density, remaining always positive. However, for $\lambda_d > 8$ the chemical potential changes signs at some critical value of the density. Since we are mostly interested in the case where the chemical potential changes sign, we choose for definiteness $\lambda_d = 8.2$. This sign change will have important consequences throughout the paper in the *d*-wave case.

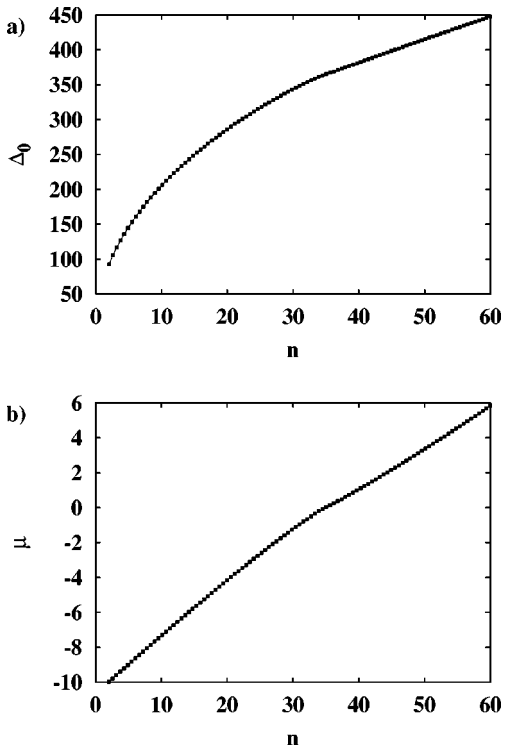

FIG. 1. (a) The order parameter Δ_{0d} and (b) the chemical potential μ as a function of density at fixed interaction $\lambda_d = 8.2$ and $k_1 = k_0 = 10$ in the *d*-wave channel. Notice that the chemical potential μ changes sign at $n = 34.85$.

When $\lambda_d = 8.2$ the BCS regime is reached for extremely high densities only. In the BCS limit ($\zeta \ll 1$) the amplitude of the order parameter ($\phi = 0$) can be calculated analytically at $k_\mu = \sqrt{2m\mu}$:

$$\Delta_l(k_\mu) \sim \exp\{2[\lambda_{0l}^{-1}(k_\mu) - \lambda_l^{-1}]/h_l^2(k_\mu)\}.$$

With our choice of $h_l(k)$, $\lambda_{0d}(k_\mu) \simeq 8 + \mu/24\epsilon_1 + \mathcal{O}([\mu/\epsilon_1]^2)$, valid for $\mu/\epsilon_1 \ll 1$, where $\epsilon_1 = k_1^2$. The ratios between $\Delta_l(k_\mu)$ and the critical temperature T_{cl} satisfy the usual relations $\Delta_s(k_\mu)/T_{cs} = 1.76$ and $\Delta_d(k_\mu)/T_{cd} = 2.14$. Similar plots can also be made for varying interaction λ_d and fixed density n. These plots are shown in Fig. 2.

In the *d*-wave case it is not very difficult to show that for fixed interaction λ_d, $\Delta_{0d}(n)$, and $\mu(n)$ have continuous first derivatives and discontinous second derivatives as a function of n at $n = n_c$, where $\mu = 0$ (see Fig. 1). The critical density for Fig. 1 is $n_c = 34.85$. Furthermore, for fixed density n, $\Delta_{0d}(\lambda_d)$, and $\mu(\lambda_d)$ have continuous first derivatives and discontinuous second derivatives as a function of λ_d at λ_d

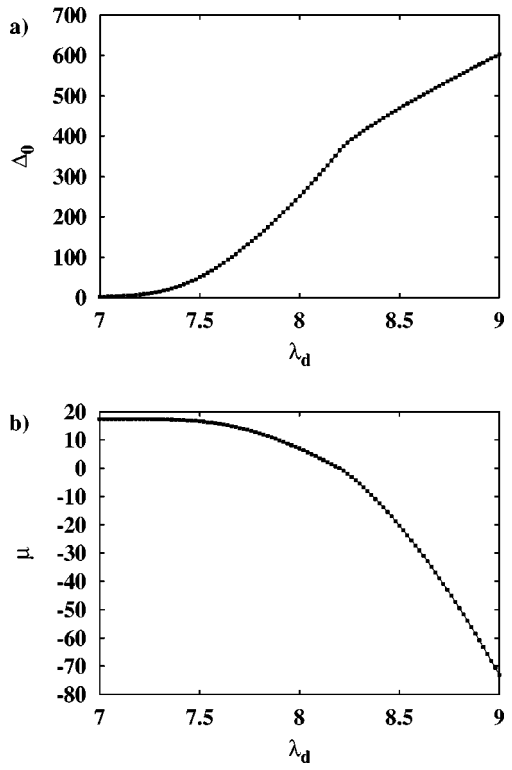

FIG. 2. (a) The order parameter Δ_{0d} and (b) the chemical potential μ as a function of coupling λ_d at fixed density $n=34.85$ and $k_1=k_0=10$ for the d-wave channel. Notice that the chemical potential μ changes sign at $\lambda_d=8.2$.

$=\lambda_{d_c}$, where $\mu=0$ (see Fig. 2). The critical interaction for Fig. 2 is $\lambda_{d_c}=8.2$. In the s-wave case, the parameters Δ_{0s} and μ have continuous first and second derivatives for all values of λ_s and n, thus at $\mu=0$ nothing special happens. However, for a d-wave system the line $\mu=0$ is very special as it will be seen in Secs. IV and V, where the quasiparticle excitation spectrum and momentum distribution are discussed, respectively.

IV. QUASIPARTICLE EXCITATION SPECTRUM AND PHASE DIAGRAM

The first important spectroscopic quantity to be analyzed is the single quasiparticle excitation spectrum $E_l(\mathbf{k})$, defined in Eq. (9). Let us discuss first the s-wave case in the zero range interaction limit $k_0\to\infty$. For $\mu>0$ the excitation spectrum has a gap at $k=k_\mu$, $E_g(k_\mu)=|\Delta_s(k_\mu)|$. This gap is completely isotropic in the vicinity of k_μ. At the intermediate regime, when $\mu=0$, the gap takes the value $E_g(0)=|\Delta_s(0)|$, when the chemical potential becomes negative towards the BEC limit, the minimum of the energy gap remains at $\mathbf{k}=0$, $E_g(0)=[\mu^2+|\Delta_s(0)|^2]^{1/2}$. When k_0 is finite the position of the minimum gap changes, but the excitation spectrum is always gapped for all values of μ. The line $\mu=0$ for the s-wave case is shown in Fig. 4(a).

In the d-wave case the situation is qualitatively different. For $\mu>0$, including the BCS limit, the excitation spectrum is gapless at k_μ along the special directions $\phi=\pm\pi/4$, $\pm 3\pi/4$, near which the excitation spectrum disperses linearly with momentum. The energy gap at $k=k_\mu$ and $\phi=0$,

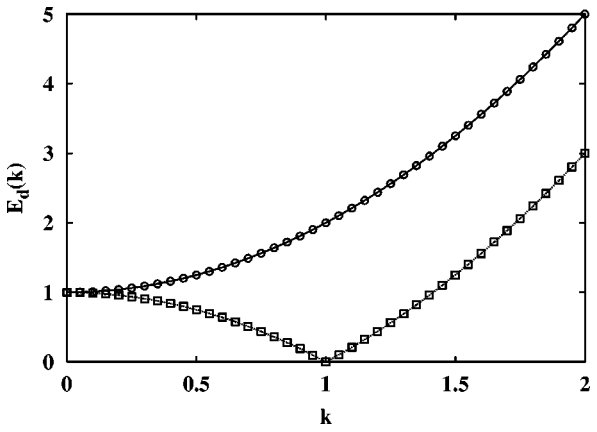

FIG. 3. The excitation spectrum $E_d(\mathbf{k})$ along $\phi=\pi/4$, for $\lambda_d=8.2$, $k_0=k_1=10$. Notice that there is no gap for $\mu>0$, but a full gap develops for $\mu<0$. The curve with no gap in the excitation spectrum (squares) corresponds to $\mu=+1.0$ ($n=39.77$), while the curve with a gap in the excitation spectrum (circles) corresponds to $\mu=-1.0$ ($n=30.83$).

$E_g(k_\mu)=|\Delta_d(k_\mu)|$ is a nonmonotonic function of k_μ for fixed density, and thus a nonmonotonic function of λ_d. The maximum $E_g(k_\mu)$ is reached at intermediate values of $\mu>0$. At $\mu=0$, the minimal gap is $E_g(0)=|\Delta_d(0)|=0$, and occurs at the single point $\mathbf{k}=0$. In this case the excitation spectrum is

$$E_d(\mathbf{k})=[\epsilon_\mathbf{k}^2+|\Delta_d(\mathbf{k})|^2]^{1/2}, \tag{10}$$

which behaves quadratically for small momenta at any given angle ϕ, since $\Delta_d(\mathbf{k})\sim k^2\cos(2\phi)$ and $\epsilon_\mathbf{k}=k^2/2m$. The shrinking of the energy gap to zero at $\mathbf{k}=0$ is a consequence of the diminishing pairing interaction $h_d(k_\mu)$ for $\mu\to 0$. As soon as $\mu<0$, including the BEC limit, a full gap in the excitation spectrum appears, but the minimal gap remains at $\mathbf{k}=0$ with value $E_g(0)=|\mu|$ since $\Delta_d(0)=0$. Thus, the $\mu=0$ line separates a gapless d-wave superconductor ($\mu>0$) from a fully gapped d-wave superconductor ($\mu<0$). The excitation spectrum $E_d(\mathbf{k})$ is shown in Fig. 3 along $\phi=\pi/4$. Notice the appearance of a full gap as the critical density n_c (where $\mu=0$) is approached from $n>n_c$ ($\mu>0$). This generic behavior allows us to construct phase diagrams in Figs. 4(b) and 4(c). The solid line corresponds to $\mu=0$ on the graph of n vs λ_d. Notice in Figs. 4(b) and 4(c) that a change in k_1 just rescales the value of λ_d by k_1^4, i.e, only renormalizes the magnitude of the interaction in the d-wave channel. So, from now on, we fix the values k_0 and k_1 to $k_0=k_1=10$, since the dependence of physical properties on k_1 can be retrieved by the scaling $\lambda_d\to\lambda_d/k_1^4$.

Notice in Fig. 4(a) that, at very low densities, an s-wave system can have negative chemical potential for arbitrarily small interactions λ_s, which can be interpreted as indicative of the appearance of a two-body bound state at arbitrarily small λ_s. On the other hand, the low density limit of a d-wave system is qualitatively different [see Figs 4(b) and 4(c)]: the chemical potential does not become negative until a critical coupling λ_{d_c} is reached. This indicates that the appearance of a two-body bound state in the d-wave state requires finite λ_d.

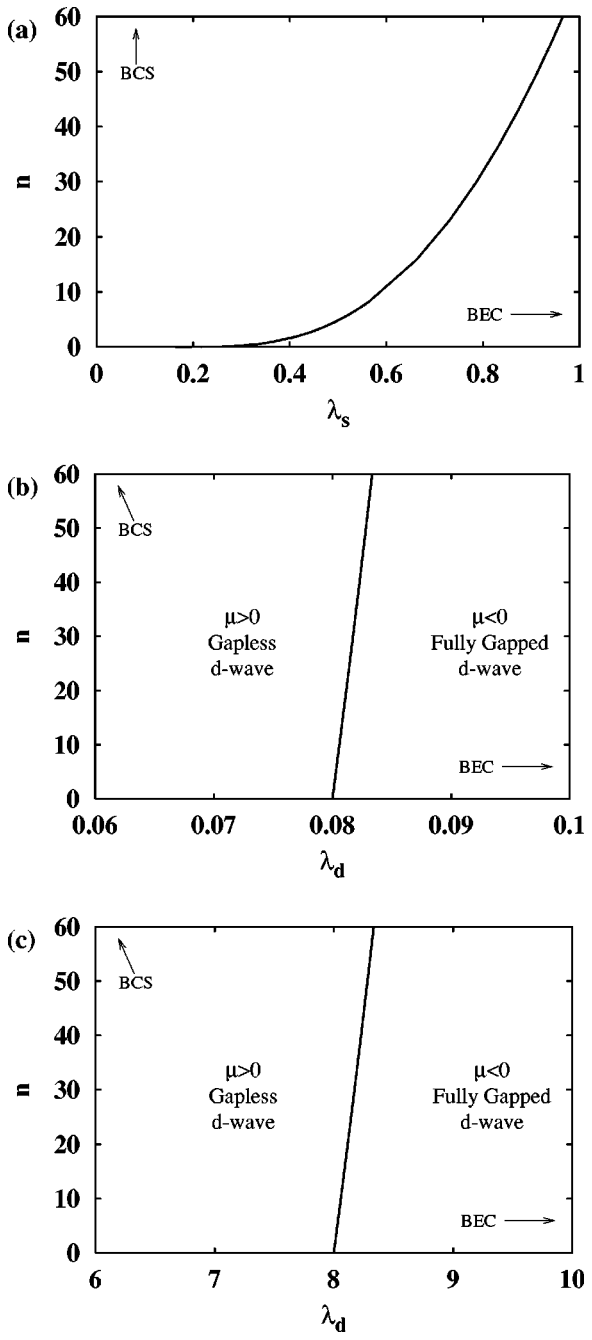

FIG. 4. Phase diagram for (a) an *s*-wave superconductor with $k_0=10$, the solid line corresponds to $\mu=0$; (b) a *d*-wave superconductor with $k_0=10$ and $k_1=\sqrt{10}$; and (c) a *d*-wave superconductor with $k_0=k_1=10$. In the *d*-wave case, the solid line ($\mu=0$) separates two different regimes: gapless for $\mu>0$ and fully gapped for $\mu<0$.

We note, in passing, that the effect discussed here (appearance of a full gap in a *d*-wave superconductor) is quite different from the effect discussed by Volovik[20] in the context of superfluid ^{3}He (a triplet *p*-wave system). In superfluid ^{3}He the appearance of the gap in the *A* phase to the *B* phase transition seems to be associated with the disappearance of nodes at the Fermi surface, as the interaction parameter changes. In ^{3}He there is always a well defined Fermi surface in the normal state, the Fermi system is highly degenerate, and pairing occurs in momentum space. The structure of the order parameter changes as the ^{3}He goes from the *A* to the *B* phase. However, during the BCS to BEC evolution for a *d*-wave superconductor, the structure of the order parameter does not change, and the appearance of the gap is strongly connected with the degeneracy of the Fermi system, i.e., pairing is becoming more local as the particle density is reduced for fixed interaction strength, or as the interaction strength is increased for fixed density of particles.

The behavior of $E_l(\mathbf{k})$ as function of μ determines the absence or presence of a gap in the quasiparticle excitation spectrum, which in turn allows us to construct the density versus interaction phase diagram presented in Fig. 4. At this point it is important to mention the work of den Hertog[15] and Andrenacci *et al.*[16] where a density versus interaction phase diagram was constructed for the lattice case using an extended Hubbard model with attraction between nearest neighbor sites. Their phase diagram contains lines that separate the qualitative behavior between BCS and BEC indicating only a crossover between the two regimes even in the *d*-wave case. Our saddle point phase diagram, however, indicates the existence of a quantum phase transition separating a gapless *d*-wave phase (BCS-like) from a fully gapped *d*-wave phase (BEC-like), as supported by the calculations presented in Secs. V through X. So, we expect a similar behavior to occur in the lattice case, since a full gap also appears when the chemical potential goes below a critical value μ_c. This possible quantum phase transition in the lattice case has not been reported in the recent literature.[15,16] The change in behavior of the excitation spectrum (from gapless to fully gapped) has also important consequences on the momentum distribution $n_l(\mathbf{k})$ at zero temperature to be discussed next.

V. MOMENTUM DISTRIBUTION

We are interested in the momentum distribution for a *d*-wave superconductor, but we also briefly discuss the *s*-wave case for comparison. The momentum distribution at low momenta can be analyzed in three different regimes $\mu>0$, $\mu=0$, and $\mu<0$.

In the *s*-wave case, for $\mu>0$, the momentum distribution is $n_s(k_\mu+\delta k)\simeq[1-2k_\mu\delta k/\Delta_s(k_\mu)]/2$ near k_μ. At low k, however, it is $n_s(k)\simeq[1+\gamma_p(1+\alpha k/2k_0)]/2$, where $\gamma_p=\mu/\sqrt{\mu^2+\Delta_{0s}^2}$, and $\alpha=\Delta_s^2/(\mu^2+\Delta_{0s}^2)$.

When $\mu=0$, the momentum distribution at small momenta is $n_s(k)\simeq(1-k^2/\Delta_{0s})/2$. For negative μ, $n_s(k)=[1-\gamma_n(1+\alpha k/2k_0)]/2$ for small k, with $\gamma_n=|\mu|/\sqrt{\mu^2+\Delta_{0s}^2}$. Notice that $n_s(0)$ is a continuous function of μ. In fact $n_s(k)$ is a smooth function of μ for all momenta. However, this is not the case for a *d*-wave system, which we shall discuss next.

The momentum distribution in the *d*-wave case is anisotropic, being $n_d(k)=[1-\mathrm{sgn}(k^2-\mu)]/2$ along the direction of the nodes ($\phi=\pm\pi/4,\pm3\pi/4$). This behavior already signals discontinuity of $n_d(k)$ as a function of μ at $k=0$, a suspicion further confirmed by analyzing the more interesting direction $\phi=0$ and its equivalents $\phi=\pm\pi/2,\pi$. Near k_μ the momentum distribution is $n_d(k_\mu+\delta k)\simeq[1-2k_\mu\delta k/\Delta_d(k_\mu)]/2$. On the other hand, the momentum distribution behaves as $n_d(k)\simeq1-(\Delta_{0d}^2/\mu^2)(k^4/4k_1^4)$ for very

small momenta k. When the chemical potential vanishes the momentum distribution at $k=0$ becomes

$$n_d(0) \simeq (1-\nu)/2, \tag{11}$$

where $\nu=(1+\Delta_{0d}^2/k_1^4)^{-1/2}$. Finally, when μ becomes negative $n_d(k) \simeq (\Delta_{0d}^2/\mu^2)(k^4/4k_1^4)$ for small k. Notice the discontinuity of the momentum distribution at low k, when the chemical potential crosses zero. This discontinuity, which is illustrated in Fig. 6 and proven analytically in Eq. (11), coincides with the collapse of the four Dirac points to a single point at $k_\mu=0$, and with the appearance of a full gap as soon as $\mu<0$. In Fig. 5 we show three-dimensional plots of the momentum distribution and corresponding contour plots, which indicate first the collapse of the four Dirac points as μ crosses zero and second a major rearrangement of the momentum distribution as soon as μ becomes negative.

This major rearrangement of the momentum distribution and the discontinuity at zero momentum has been noted before by Borkowski and Sá de Melo[14] in the continuum case and by den Hertog[15] in the lattice case. This particular behavior of the momentum distribution in the d-wave case has a dramatic effect in the compressibility, which is discussed next.

VI. COMPRESSIBILITY

In the s-wave case, the ground state energy is a smooth function of μ, and does not present any anomalous behavior in the vicinity of $\mu=0$. Furthermore, the ground state energy is a smooth function of both λ_s and density n. The first and second derivatives of the ground state energy with respect to the chemical potential μ are well behaved, and so is the compressibility of the s-wave system. This is expected since the evolution of the ground state from the BCS limit to the BEC limit is smooth for the s-wave case.[11] On the other hand, for the d-wave case the ground state energy changes dramatically around $\mu=0$. The ground state energy is always continuous, and has continuous first derivatives, but its second derivative with respect to μ is proportional to the isothermal compressibility

$$\kappa = \frac{1}{n^2}\frac{dn}{d\mu}. \tag{12}$$

The previous expression can be rewritten in a more elegant form

$$\kappa = 4n^{-2}\sum_{\mathbf{k}} \varphi_l^*(\mathbf{k}) E_l^{-1}(\mathbf{k}) \varphi_l(\mathbf{k}), \tag{13}$$

where $\varphi_l(\mathbf{k})=\Delta_l(\mathbf{k})/2E_l(\mathbf{k})$ is the bound state wave function for the lth angular momentum state.

The compressibility κ diverges logarithmically in the vicinity of $\mu=\mu_c=0$ for the d-wave case. This result is not surprising given that when the chemical potential crosses zero a full gap to addition of quasiparticles suddenly appears. Thus, the compressibility of the system diverges at $\mu_c=0$, when $n=n_c$, suggesting the existence of a quantum critical point. In the vicinity of $\mu=0$, the density $n-n_c \approx -\beta_1 \mu \ln|\mu| + \beta_2 \mu$, and the compressibility is

$$\kappa \approx [-\beta_1 \ln|n-n_c| + \beta_2]/n^2, \tag{14}$$

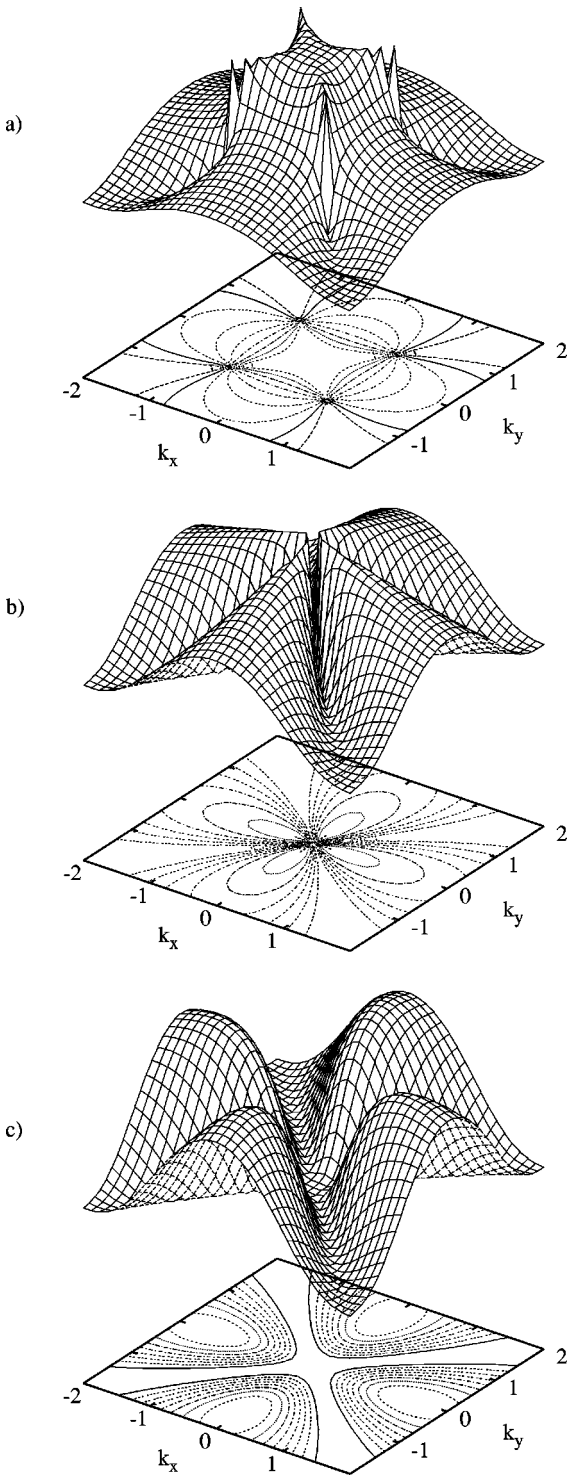

FIG. 5. Three-dimensional and contour plots of the momentum distribution for $\lambda_d=8.2$, $k_1=k_0=10$ and a d-wave order parameter (a) $\mu=+1.0, n=39.77$, (b) $\mu=0, n=n_c=34.85$, (c) $\mu=-1.0, n=30.83$. Notice in (a) the presence of the four Dirac points in the contour plots of $n_d(\mathbf{k})$, and how these points collapse in (b) leading to a major redistribution of $n_d(\mathbf{k})$ in (c).

where the constant β_2 depends only on the sign of μ (or sign of $n-n_c$). See this asymmetry in Fig. 7.

The singular behavior of the compressibility indicated in Fig. 7 combined with the appearance of a full gap in the excitation spectrum indicates a possible quantum phase transition. The fact that the compressibility diverges is intimately

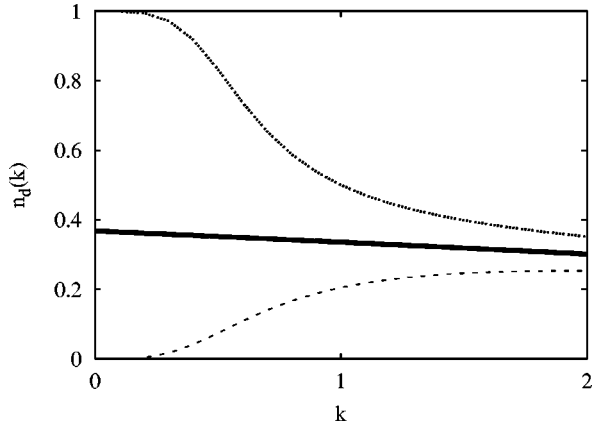

FIG. 6. The momentum distribution of quasiparticles for $\phi=0$, $\lambda_d=8.2$, $k_1=k_0=10$, and several values of $\mu=+1.0,0,-1.0$ for a *d*-wave order parameter. The dotted line indicates the case where $n>n_c$ and the chemical potential $\mu>0$ ($\mu=+1.0$). Notice that the momentum distribution $n_d(0)=1$. The dashed line indicates the case where $n<n_c$, $\mu<0$ ($\mu=-1.0$), and $n_d(0)=0$. The solid line indicates the case where $n=n_c$, $\mu=0$. Notice the discontinuity of $n_d(0)$, confirming the analytical result of Eq. (11).

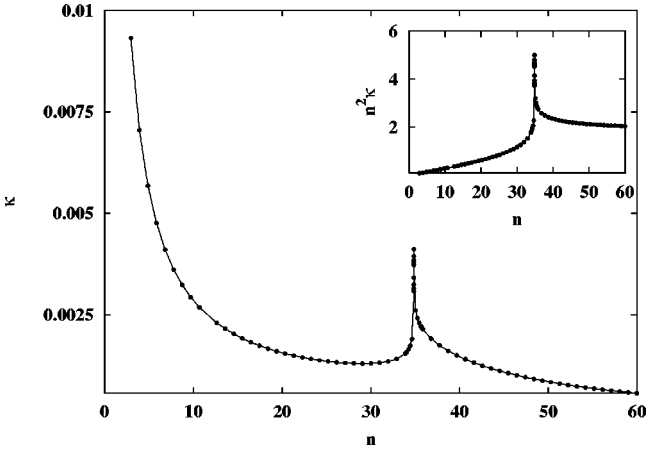

FIG. 7. The compressibility κ for *d*-wave order parameters as a function of density *n*, but fixed interaction parameters $\lambda=8.2$, $k_1=k_0=10$. Notice the divergence of κ when $n=n_c=34.85$, and the asymmetry of κ in the immediate vicinity of $n=n_c$.

associated with divergences in the spatiotemporal correlations, which are discussed next.

VII. DENSITY-DENSITY CORRELATIONS

Diverging correlation lengths are a characteristic feature of classical critical points, but quantum critical points involve divergences in correlation lengths and times. A measure of correlations in the ground state can be obtained by analyzing the zero time ($\tau=0$) opposite spin density-density correlation function

$$\mathcal{F}^{(l)}_{\uparrow\downarrow}(\mathbf{r},\mathbf{r}',\tau=0)=\langle G_l|n_\uparrow(\mathbf{r})n_\downarrow(\mathbf{r}')|G_l\rangle-\mathcal{N}^{(l)}_{\uparrow\downarrow}(\mathbf{r},\mathbf{r}') \tag{15}$$

where $n_\sigma(\mathbf{r})=\psi^\dagger_\sigma(\mathbf{r})\psi_\sigma(\mathbf{r})$ is the particle density at position $\mathbf{r}$, and $\mathcal{N}^{(l)}_{\uparrow\downarrow}(\mathbf{r},\mathbf{r}')=\langle G_l|n_\uparrow(\mathbf{r})|G_l\rangle\langle G_l|n_\downarrow(\mathbf{r}')|G_l\rangle$. The correlation function above can expressed as

$$\mathcal{F}^{(l)}_{\uparrow\downarrow}(\mathbf{r}-\mathbf{r}')=\left|\frac{1}{\mathcal{V}}\sum_{\mathbf{k}}\varphi_l(\mathbf{k})\exp[-i\mathbf{k}\cdot(\mathbf{r}-\mathbf{r}')]\right|^2, \tag{16}$$

in terms of the bound state wave function $\varphi_l(\mathbf{k})$ for the *l*th angular momentum state.

This correlation function can be easily calculated in the long wavelength limit. In the *s*-wave case $\mathcal{F}^{(s)}_{\uparrow\downarrow}(\rho)\propto|\rho|^{-4}$ for all values of μ, where $\rho=|\mathbf{r}-\mathbf{r}'|$. Nothing special occurs when $\mu=0$, as can read off from the *s*-wave correlation length $\xi^{(s)}(\theta)=[A_s\Delta_s^2/(\mu^2+\Delta_s^2)]^{1/4}$, i.e., the correlation length is finite for all μ, and independent of the angle θ. Here A_s is a constant. The situation is different in the *d*-wave case where $\mathcal{F}^{(d)}_{\uparrow\downarrow}(\rho,\theta)\propto A_d(\theta)/\rho^8$, and the *d*-wave density-density correlation length is

$$\xi^{(d)}(\theta)=\left[\frac{\Delta_d^2}{k_1^4\mu^2}A_d(\theta)\right]^{1/8}, \tag{17}$$

where $A_d(\theta)=a_{d_1}\cos^2(2\theta)+a_{d_2}\sin^2(2\theta)$. Here a_d's are numerical constants, which reflect the strong dependence of $\xi^{(d)}$ on the direction θ. This indicates that the correlation length diverges as $|\mu-\mu_c|^{-1/4}$, where $\mu_c=0$. Thus, opposite spin density-density correlations get strongly enhanced near $\mu=\mu_c$. Exactly at $\mu=\mu_c=0$, the correlation function is

$$\mathcal{F}^{(d)}_{\uparrow\downarrow}(\rho,\theta)=\left(\frac{k_{F_{\max}}}{2\mathcal{V}}\right)^2\left[\frac{\Delta_d}{k_1^2}\right]^2\frac{B_d(\theta)}{\rho^4}, \tag{18}$$

where $B_d(\theta)$ is some function of θ. From this expression we can extract the critical exponent $\eta=1/4$.

To determine the divergent time scale it is necessary to look at the time dependent opposite spin density-density correlation function $\mathcal{F}^{(l)}_{\uparrow\downarrow}(\mathbf{r},\mathbf{r}',\tau)$, where $n_\sigma(\mathbf{r})$ is replaced by $n_\sigma(\mathbf{r},\tau)=\exp(-H\tau)n_\sigma(\mathbf{r})\exp(H\tau)$ in Eq. (15). Near $\mu=0$, the Fourier transform of $\mathcal{F}^{(l)}_{\uparrow\downarrow}(\mathbf{r},\mathbf{r}',\tau)$ is proportional to $\exp(-|\mu|\tau)$ ($\hbar=1$) in the long wavelength limit $\mathbf{k}\to0$. This indicates that the correlation time $\xi_\tau=|\mu|^{-1}$, i.e., the dynamical scaling exponent $z=4$. We reserve a detailed analysis of the critical phenomena of this new quantum phase transition, beyond the saddle point approximation discussed here, for a later opportunity.[21] Possible low-temperature phase diagrams are schematically drawn in Fig. 8.

We would like to mention, however, that this superconductor-superconductor *quantum* phase transition is similar to the *classical* liquid-gas phase transition in the sense that it occurs without a change in symmetry,[22] but the coexistence region is completely suppressed in the present case, since the critical point (μ_c,T_c) is pushed all the way down to the origin of the μ vs T phase diagram. So the transition should be continuous, and the energy gap E_g for quasiparticle excitations is playing the role of the *order parameter*: $E_g=0$ for $n>n_c$, while $E_g>0$ for $n<n_c$, as can be seen indicated in Fig. 9. Thus strictly in two spatial dimensions, one should expect a finite temperature phase diagram of the type indicated in Fig. 8(a), since the Mermin-Wagner-Berezinskii theorem would predict the absence of finite temperature long-range order in two-dimensional systems with a continuous symmetry.[23–25] For higher spatial dimensions, phase diagrams indicated in Figs. 8(b) and 8(c) are additional possibilities.

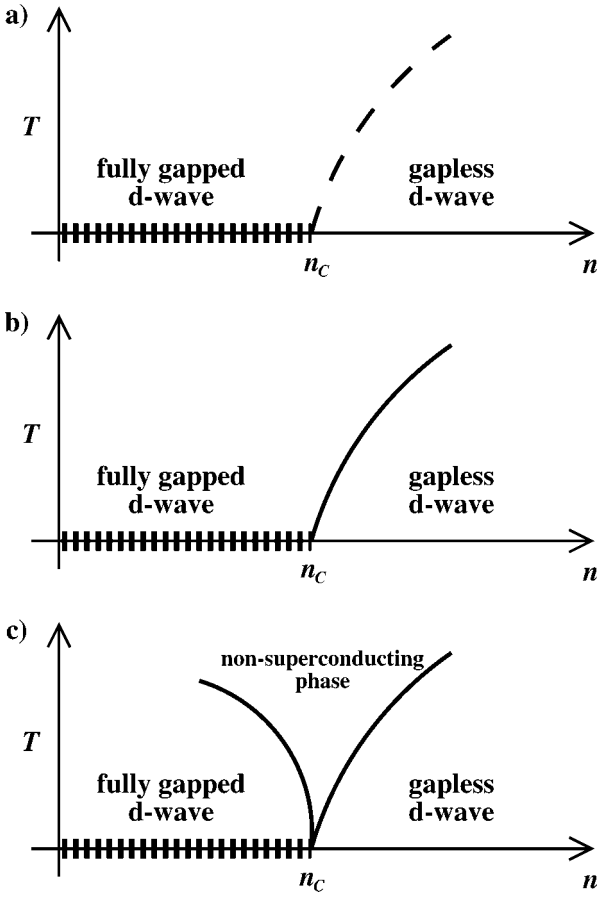

FIG. 8. (a) Shows a phase diagram where a fully gapped *d*-wave phase is present at lower densities and a gapless *d*-wave phase is present at higher densities and the critical point occurs only at $n=n_c$ and $T=0$. At finite temperatures there is only a crossover. (b) Indicates that there can be a finite temperature phase boundary between the fully gapped and the gapless *d*-wave phases, terminating at the quantum critical point n_c. (c) Shows a schematic phase diagram where at finite temperatures the fully gapped *d*-wave phase at higher densities becomes first nonsuperconducting and then gapless *d*-wave as the density is increased further.

The changes in the momentum distribution and in the excitation spectrum not only affect the compressibility of the system and the opposite spin density-density correlation function as discussed above, but also affect the Cooper pair size to be discussed next.

VIII. COOPER PAIR SIZE

The Cooper pair size in the saddle point approximation is given by

$$[\xi_{\rm pair}^{(l)}]^2 = -\frac{\int d^2\mathbf{k}\,\varphi_l^*(\mathbf{k})\nabla_k^2\varphi_l(\mathbf{k})}{\int d^2\mathbf{k}\,\varphi_l^*(\mathbf{k})\varphi_l(\mathbf{k})}, \tag{19}$$

In Figs. 10 and 11 we see plots of the Cooper pair size for both *d*- and *s*-wave cases for fixed interaction strength and changing density or fixed density and changing interaction strength.

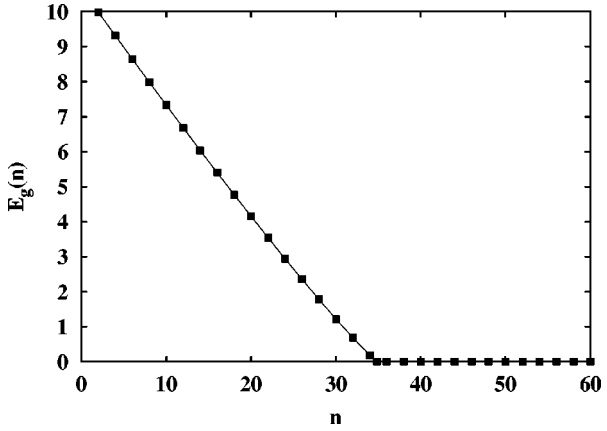

FIG. 9. The energy gap as a function of density for a *d*-wave superconductor with $\lambda_d=8.2$ and $k_1=k_0=10$. The gap disappears for $n\geqslant n_c=34.85$.

Notice that in the *s*-wave case the pair size is a monotonically increasing function of density for fixed interaction strength [Fig. 11(a)], and a monotonically decreasing function of interaction strength for fixed density [Fig. 11(b)]. However, in the *d*-wave case the pair size first increases as a function of density [Fig. 10(a)] for $n<n_c$, diverges at $n=n_c$ when the chemical potential crosses zero, and decreases for $n>n_c$. This divergence of the pair size occurs always when the line $\mu=0$ is crossed in the density versus interaction phase diagram [see phase diagram in Figs. 4(b) and 4(c)]. A similar divergence occurs also for fixed density and changing interaction strength as seen in Fig. 10(b). *Prima facie* divergences in $\xi_{\rm pair}^{(d)}$ seem to suggest unbinding of the Cooper pairs at n_c, which (in two spatial dimensions) would favor a finite temperature phase diagram of the type described in Fig. 8(a). This divergence in $\xi_{\rm pair}^{(d)}$ is present only when the chemical potential μ changes sign. For instance, if the interaction strength is too small $\lambda_d<\lambda_{d_c}$ [see phase diagram in Figs. 4(b) and 4(c)], μ does not change sign as function of density, and thus no divergence in $\xi_{\rm pair}^{(d)}$ occurs.

In the lattice case Andrenacci *et al.* have noticed that their $\xi_{\rm pair}$ for a *d*-wave solution had a peculiar behavior as a function of the nearest-neighbor interaction $|V|$ when n approached half filling. They found that $\xi_{\rm pair}$ does not show a monotonic decrease for increasing $|V|$ and converges asymptotically (when $|V|\to\infty$ and $n<1$) to a finite value which is larger than the lattice spacing. They argue that the divergence in $\xi_{\rm pair}$ is due to the establishment of quasi-long-range-order correlations among the composite bosons, which reside individually on nearest neighbors sites. We suspect, in addition to the results of Andrenacci *et al.*,[16] that a quantum phase transition should occur also in lattice models when $\mu=\mu_c$, i.e., for interaction strength and varying density or vice versa. Having considered several signatures of this possible phase transition, we now turn our attention to its topological nature.

IX. A TOPOLOGICAL TRANSITION

We have already established that the transition from the BCS-like state to the BEC-like state occurs without changing the symmetry of the order parameter (Sec. VII) in *d*-wave systems. If the symmetry is not changing at the transition

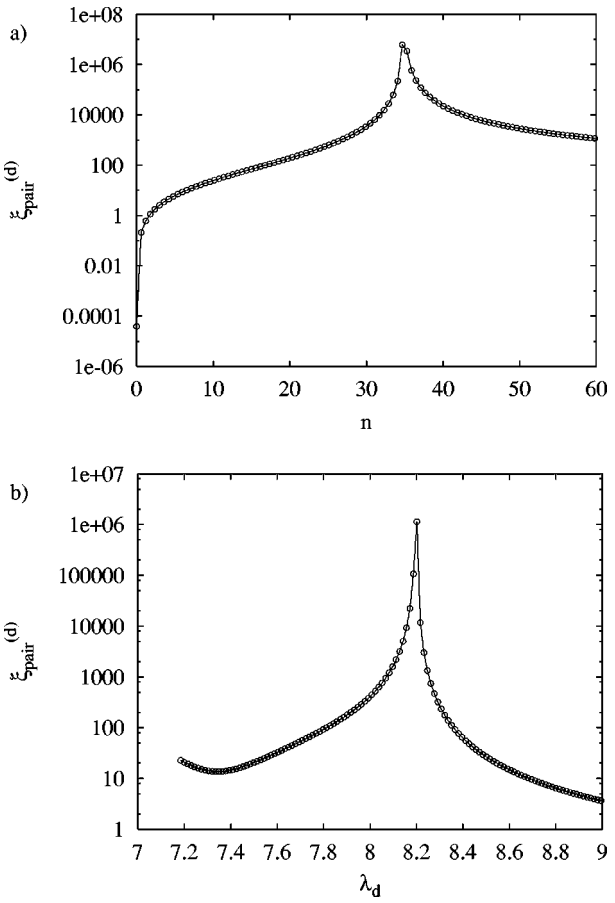

FIG. 10. The pair size $\xi^{(d)}_{\rm pair}$ for a *d*-wave superconductor with $k_1=k_0=10$: (a) $\xi^{(d)}_{\rm pair}$ as a function of density n for $\lambda_d=8.2$; (b) $\xi^{(d)}_{\rm pair}$ as a function of interaction strength λ_d for $n=34.85$.

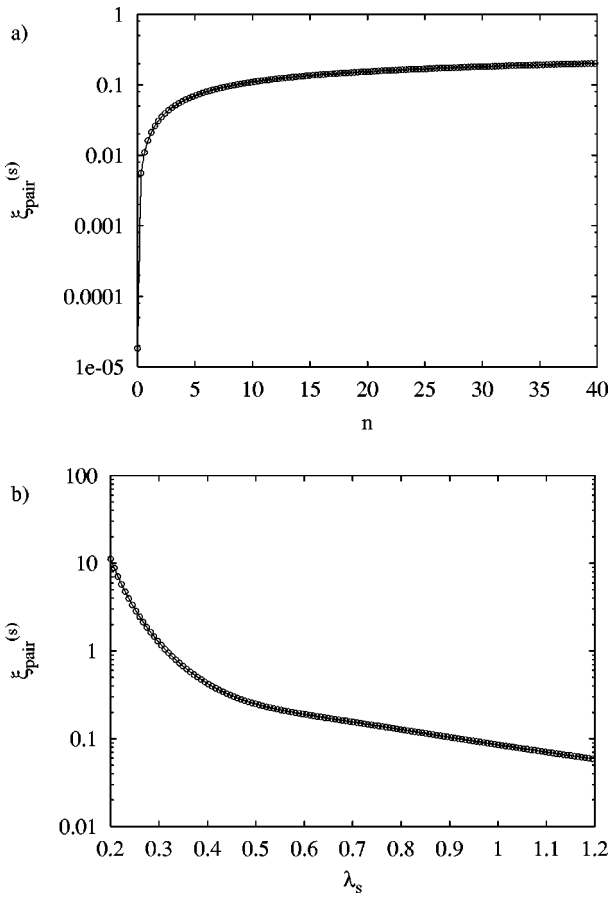

FIG. 11. The pair size $\xi^{(s)}_{\rm pair}$ for an *s*-wave superconductor with $k_0=10$: (a) $\xi^{(s)}_{\rm pair}$ as a function of density n for $\lambda_s=0.7$; (b) $\xi^{(s)}_{\rm pair}$ as a function of interaction strength λ_s for $n=20$.

point $\mu=0$, then what is? We will argue in the following lines that the internal topology of the ground state is changing in momentum space. The following topological considerations are inspired in the work of Volovik[20] on exotic properties of ^{3}He, a *p*-wave superfluid. The topological considerations presented here include only the saddle point approximation used throughout the manuscript.[26]

A. Ground state topological correlations

As the chemical potential passes through zero ($\mu=0$) the symmetry of the ground state does not change both in the *s*-wave case and *d*-wave case, however in the *d*-wave case gapless ($\mu>0$) excitations disappear leading to fully gapped ($\mu<0$) excitations. The compressibility of the *d*-wave system divergences at $\mu=0$ indicating that a quantum phase transition takes place when the Dirac points collapse at $\mathbf{k}=\mathbf{0}$. The disappearance of these gapless points (Dirac points) is intimately connected with the momentum space topology, so that we can give a finer classification to the *d*-wave system, and characterize the quantum phase transition at $\mu=0$ as topological in nature.

Further insight is gained by rewriting the ground state wave function $|\Psi\rangle=\Pi_{\mathbf{k}}(u_{\mathbf{k}}+v_{\mathbf{k}}\psi^{\dagger}_{\mathbf{k},\uparrow}\psi^{\dagger}_{-\mathbf{k},\downarrow})|0\rangle$ as

$$|\Psi\rangle=\prod_{\mathbf{k}}|u_{\mathbf{k}}|^{1/2}\exp\left[\frac{1}{2}\sum_{\mathbf{k}}g_{\mathbf{k}}\psi^{\dagger}_{\mathbf{k},\uparrow}\psi^{\dagger}_{-\mathbf{k},\downarrow}\right]|0\rangle, \tag{20}$$

where the functions $u_{\mathbf{k}}$ and $v_{\mathbf{k}}$ are determined up to a global phase for each momentum $\mathbf{k}$, and thus can be chosen as real having the usual form

$$u^2_{\mathbf{k}}=[1+\sin\theta_{\mathbf{k}}]/2 \tag{21}$$

and

$$v^2_{\mathbf{k}}=[1-\sin\theta_{\mathbf{k}}]/2, \tag{22}$$

where $u^2_{\mathbf{k}}+v^2_{\mathbf{k}}=1$ to guarantee the normalization of the ground state wave function $|\Psi\rangle$. The angle $\theta_{\mathbf{k}}$ is defined by

$$\cos\theta_{\mathbf{k}}=\Delta_l(\mathbf{k})/E_l(\mathbf{k}), \tag{23}$$

$$\sin\theta_{\mathbf{k}}=(\epsilon_{\mathbf{k}}-\mu)/E_l(\mathbf{k}). \tag{24}$$

In the Bogoliubov formulation the parameters $u_{\mathbf{k}}$ and $v_{\mathbf{k}}$ define the usual quasiparticle operators

$$\gamma^{\dagger}_{\mathbf{k}\oplus}=u_{\mathbf{k}}\psi^{\dagger}_{\mathbf{k}\uparrow}-v_{\mathbf{k}}\psi_{-\mathbf{k}\downarrow} \tag{25}$$

and

$$\gamma_{-\mathbf{k}\ominus}=u_{\mathbf{k}}\psi_{-\mathbf{k}\downarrow}+v_{\mathbf{k}}\psi^{\dagger}_{\mathbf{k}\uparrow}, \tag{26}$$

which diagonalize the Bogoliubov matrix defined in Eq. (32). Notice that the momentum space loci where $v_{\mathbf{k}}=0$ contains nonpaired electrons in the ground state as can be inferred from the form of the variation wave function $|\Psi\rangle$, and contains single quasiparticle excitations which do not mix spin up and spin down electrons. The parameters $u_{\mathbf{k}}$ and $v_{\mathbf{k}}$ also define a S^1 space (unit circle) with unit vector $\hat{\mathbf{d}}(\mathbf{k})=(u_{\mathbf{k}},v_{\mathbf{k}})$, thus the mapping of closed curves containing Dirac points from the two-dimensional momentum space into the unit circle defined by $u_{\mathbf{k}}$ and $v_{\mathbf{k}}$ belongs to the homotopy group $\pi_1(S^1)=Z$. For $\mu>0$ the topological map wraps around the unit circle twice and leads to a topological class with index $\tilde{d}=2$. However, for $\mu<0$, the topological map does not wrap around the unit circle at all, and belongs to a topological class with index $\tilde{d}=0$. Since it is not possible to pass from one topological class to another in a continuous manner, a topological phase transition must occur. In the *s*-wave case, however, such a transition does not occur, since the topological map is trivial, i.e., $\tilde{d}=0$ for all values of μ.

In addition, the function

$$g_{\mathbf{k}}=v_{\mathbf{k}}/u_{\mathbf{k}}=\tan\theta_{\mathbf{k}}-\sec\theta_{\mathbf{k}} \tag{27}$$

is a direct measure of the electron-electron correlations in the ground state and contains information about the topology of the ground state. Therefore, we analyze the Fourier transform of $g_{\mathbf{k}}$ [which we call $F_g(\rho,\theta)$] to extract the real space consequences of such a topological transition in momentum space. We analyze first the *d*-wave case. In the BCS-like region of the phase diagram ($\mu>0$) the correlation function

$$F_g(\rho,\theta)=\frac{\mu k_1^2}{\Delta_{0d}}f_+(\theta), \tag{28}$$

which is independent of the particle separation ρ. Notice that the prefactor vanishes as $\mu\to 0$. However, at the transition line $\mu=0$,

$$F_g(\rho,\theta)=f_0(m,k_1^2/\Delta_{0d},\theta)/\rho^2. \tag{29}$$

And finally, in the BEC-like region of the phase diagram ($\mu<0$),

$$F_g(\rho,\theta)=\left[\frac{k_1^2}{4m^2\Delta_{0d}}f_{1-}(\theta)+\frac{\Delta_{0d}}{2k_1^2}f_{2-}(\theta)\right]\Big/\,|\mu|\rho^4. \tag{30}$$

Notice that the prefactor diverges at $\mu\to 0$. Thus, the correlation function $F_g(\rho,\theta)$ has clearly three distinct behaviors: (a) it is a constant when the Dirac points exist in momentum space ($\mu>0$); (b) it is proportional to ρ^{-2} when the Dirac points collapse ($\mu=0$); (c) it is proportional to ρ^{-4} when the Dirac points do not exist ($\mu<0$). These different regimes strengthen the point of view that the ground state evolution from BCS to BEC in *d*-wave superconductors is not smooth, i.e., there is a phase transition separating the two regimes. [In the *s*-wave case the form of the correlations in the ground state remain the same for all values of μ, i.e., $F_g(\rho,\theta)\propto\rho^{-2}$ and independent of θ, which further demonstrates that in this case there is only a crossover between the BCS and BEC limits.] After analyzing the ground state topology, it is useful to investigate topological properties of the fermionic excitations, which will be important for the calculation of thermodynamic properties in Sec. X.

B. Internal topology of excited states

To elucidate the nature of the proposed transition it is essential to analyze further the fermionic excitations during the evolution from BCS to BEC superconductivity in a *d*-wave system. Therefore, it is convenient to write the reduced Hamiltonian

$$H_{\rm red}=\sum_{\mathbf{k}}\,(\psi^\dagger_{\mathbf{k}\uparrow}\psi_{-\mathbf{k}\downarrow})\overline{H}\begin{pmatrix}\psi_{\mathbf{k}\uparrow}\\ \psi_{-\mathbf{k}^\dagger\downarrow}\end{pmatrix}, \tag{31}$$

where the Bogoliubov matrix is

$$\overline{H}=\begin{bmatrix}(\epsilon_{\mathbf{k}}-\mu) & \Delta_l(\mathbf{k})\\ \Delta_l(\mathbf{k}) & -(\epsilon_{\mathbf{k}}-\mu)\end{bmatrix}. \tag{32}$$

This matrix can be written in a pseudospin form as

$$\overline{H}=E_l(\mathbf{k})\hat{\mathbf{m}}(\mathbf{k})\cdot\vec{\sigma}, \tag{33}$$

where the unit vector $\hat{\mathbf{m}}(\mathbf{k})=(\cos\theta_{\mathbf{k}},0,\sin\theta_{\mathbf{k}})$ plays the role of a two-component spinor, parametrized by a single angle $\theta_{\mathbf{k}}$ as defined in Eqs. (23) and (24).

The vector $\vec{\sigma}=\sigma_x\hat{\mathbf{k}}_x+\sigma_y\hat{\mathbf{k}}_y+\sigma_z\hat{\mathbf{k}}_z$, where σ_x, σ_y, and σ_z are just the usual Pauli matrices, and $E_l(\mathbf{k})$ is the quasiparticle excitation energy defined in Eq. (9). Since, the *d*-wave state considered here does not break time reversal symmetry, the mapping of closed curves containing Dirac points from the two dimensional (k_x,k_y) into the S^1 spinor space defined by $|\hat{\mathbf{m}}(\mathbf{k})|^2=1$ (unit circle) belongs to the homotopy group $\pi_1(S^1)=Z$, where Z is an integer. Any nontrivial map from momentum space to spinor space is labeled by an integer

$$\tilde{m}=\frac{1}{4\pi}\int_\Omega dk_x\,dk_y\,\hat{\mathbf{m}}(\mathbf{k})\cdot\frac{\partial\hat{\mathbf{m}}(\mathbf{k})}{\partial k_x}\wedge\frac{\partial\hat{\mathbf{m}}(\mathbf{k})}{\partial k_y}, \tag{34}$$

which plays the role of the topological charge and defines equivalence classes. The domain Ω contains the neighboorhood of the Dirac points, where $E_l(\mathbf{k})$ vanishes.

In the case where $\mu>0$ the mapping is nontrivial and has topological charge $\tilde{m}=2$, while when $\mu<0$ the topological charge vanishes $\tilde{m}=0$. However, it is not possible to pass from one class to another in a continuous manner, therefore there must be a ''transition'' of topological nature occurring at $\mu=0$. This topological feature in the fermionic excited states parallels the topological phase transition in the ground state. And since the Dirac points correspond to the *loci* of zero quasiparticle energy $E_l(\mathbf{k})$ it is possible to view this phenomenon as a Lifshitz transition to be discussed next.

C. Lifshitz transition

This topological ''transition'' reminds us of the Lifshitz transition in metals at high pressures, where the Fermi surface $\epsilon(\mathbf{k},P)=E_F$ changes its topology as pressure P is changed, the simplest example being when a single simply connected Fermi surface breaks into two simply connected parts at a critical pressure P_c. This type of transition affects singularly the energy dependence of the density of states of the metal, and leads to anomalies in thermodynamic and transport properties, because of the dramatic change in the electronic dispersion $\epsilon(\mathbf{k},P)$ in the vicinity of the critical pressure P_c.[27] The topological transition discussed here is analogous to the Lifshitz transition in the sense that the surface in momentum space corresponding to $E_l(\mathbf{k},\mu)=0$ changes from four Dirac points ($\mu>0$) to a single point ($\mu=0$) to a null set ($\mu<0$), where $E_l(\mathbf{k},\mu)$ plays the role of $\epsilon(\mathbf{k},P)$ and $\mu=\mu_c=0$ plays the role of the critical pressure P_c. (We note in passing that in the lattice case such a transition should also be present, since similar momentum space topological changes are also present.) In addition, the dominant contribution to the dispersion of low lying quasiparticles changes from linear ($\mu>0$) to quadratic ($\mu=0$) to a constant ($\mu<0$), as seen in Sec. IV. This in turn produces dramatic changes in thermodynamic properties just like in the usual Lifshitz transition. Thus, next we turn out attention to the changes in the spin susceptibility and specific heat at low temperatures.

X. THERMODYNAMIC QUANTITIES

To have a full picture of the evolution from BCS to Bose-Einstein condensation superconductivity at low temperatures, it is also important to analyze thermodynamic properties such as the spin susceptibility and the specific heat. For any quantities to be calculated at finite temperatures, one needs to generalize the saddle point and number equation obtained at zero temperature. We generalize the saddle point equation and number equations at low temperatures as discussed in Engelbrecht, Randeria, and Sá de Melo[12] for the case of independent angular momentum channels and obtain a BCS-like thermodynamic potential Ω_0, which upon minimization with respect to $v_{\mathbf{k}}$ leads to the gap equation

$$\Delta_l(\mathbf{k})=-\sum_{\mathbf{k}'} V^{(l)}_{\mathbf{k},\mathbf{k}'}\frac{\Delta_l(\mathbf{k}')}{2E_l(\mathbf{k}')}\Gamma_{\mathbf{k}'}(T). \tag{35}$$

The particle density is fixed by $n_0=-\partial\Omega_0/\partial\mu$ and corresponds to the expression

$$n_0=2\sum_{\mathbf{k}} n_l(\mathbf{k},T), \tag{36}$$

where the temperature dependent momentum distribution is

$$n_l(\mathbf{k},T)=v^2_{\mathbf{k}}+(u^2_{\mathbf{k}}-v^2_{\mathbf{k}})f[E_l(\mathbf{k})]. \tag{37}$$

The set of equations discussed above is valid only for temperatures $T\ll T_c$ since the thermodynamic potential Ω_0 does not include collective modes of the system, which have been shown to be very important in the vicinity of T_c.[11,12] Furthermore, even at low temperatures the collective modes contribute to the thermodynamic potential as pointed out in Ref. 12. The thermodynamic potential then becomes

$$\Omega=\Omega_0+\Omega_{\rm col}, \tag{38}$$

where the contribution from collective modes is

$$\Omega_{\rm col}=T\sum_{\mathbf{q}} \ln\{1-\exp[\omega(\mathbf{q})/T]\}. \tag{39}$$

For a neutral superfluid at low temperatures ($T\ll T_c$), the low-energy collective modes dominate. They correspond to the Goldstone modes with frequency $\omega(\mathbf{q})=c_l(\theta)|\mathbf{q}|$ at small wave vectors $\mathbf{q}$ for all values of μ. However, in the case of a charged superfluid residual Coulomb interactions are important and these modes are plasmonized, i.e., a gap appears in their excitation spectra. These collective excitation corrections change the number equation to

$$n=n_0+n_{\rm col}, \tag{40}$$

where $n_{\rm col}=-\partial\Omega_{\rm col}/\partial\mu$. The effects of these corrections are discussed next in the cases of the spin susceptibility and specific heat.

A. Spin susceptibility

The main contribution to the spin susceptibility comes from quasiparticle excitations since they carry spin. The collective modes are *spinless* (neutral or charged) bosonic excitations, and do not affect substantially the spin dependent response. As a consequence the spin susceptibility takes the form

$$\chi_l(T)=-2\mu_e^2\sum_{\mathbf{k}}\frac{\partial f[E_l(\mathbf{k})]}{\partial E_l(\mathbf{k})}, \tag{41}$$

which can be rewritten as

$$\chi_l(T)=2\mu_e^2\int_0^\infty\frac{d\omega}{T}\tilde{N}_l(\omega)\frac{\exp(\omega/T)}{[1+\exp(\omega/T)]^2}, \tag{42}$$

where $\tilde{N}_l(\omega)=\Sigma_{\mathbf{k}}\delta(\omega-E_l(\mathbf{k}))$ is an auxiliary density function not to be confused with the real density of states of the system. A simple redefinition of variables $x=\omega/T$ indicates that $\chi_d(T)$ is controlled by the low frequency behavior of $\tilde{N}_d(\omega)$, which quite generally has the form

$$\tilde{N}_d(\omega)=\rho_{2D}\begin{cases}\alpha\omega, & \text{when} \quad \mu>0,\\ \beta, & \text{when} \quad \mu\to 0^{\pm},\\ \gamma g(\omega)\Theta(\omega-|\mu|), & \text{when} \quad \mu<0.\end{cases} \tag{43}$$

The coefficients α, β, and γ depend on μ and Δ_{0_d}, thus for a given coupling strength λ_d, they depend on the interaction range k_0 and density n. This behavior of $\tilde{N}_d(\omega)$ leads to the following behavior of the susceptibility for the *d*-wave system

$$\chi_d(T)=2\mu_e^2\rho_{2D}\begin{cases}\alpha T\ln(2), & \text{when} \quad \mu>0,\\ \beta/2, & \text{when} \quad \mu\to 0^{\pm},\\ \gamma g(|\mu|,T)\exp-[|\mu|/T], & \text{when} \quad \mu<0.\end{cases} \tag{44}$$

The result for $\mu<0$ above is valid only for $|\mu|/T\gg 1$. Notice the qualitative change in the spin susceptibility at low temperatures as μ aproaches zero. For instance, the fact that the susceptibility is finite when $\mu\to 0$ and $T\to 0$ is indicative that there exist unpaired spins in the ground state that can respond to an external magnetic field. This observation is consistent with the divergence of $\xi_{\rm pair}^{(d)}$ found in Sec. VIII, and with gapless quasiparticle excitations with a quadratic dispersion relation as found in Sec. IV. Furthermore, notice a discontinuity in the slope of $\chi_d(T)$ when $T\to 0$ and $\mu\to 0$. All these observations support the idea that a quantum phase transition occurs at $\mu=0$ and $T=0$. Similar qualitative behavior occurs also in the specific heat to be discussed next.

B. Specific heat

There are several contributions to the low temperature specific heat. We will discuss here only the contribution from quasiparticles and collective modes. The contribution from quasiparticles is

$$C_l(T)=2\sum_{\mathbf{k}} E_l(\mathbf{k})\frac{\partial f[E_l(\mathbf{k})]}{\partial T}, \tag{45}$$

which can be rewritten as

$$C_l(T)=2T\int_0^\infty \frac{d\omega}{T}\tilde{N}_l(\omega)\left(\frac{\omega}{T}\right)^2\frac{\exp(\omega/T)}{[1+\exp(\omega/T)]^2}. \tag{46}$$

The behavior of $\tilde{N}_d(\omega)$ at low frequencies translates into the following low temperature dependence of the quasiparticle specific heat for the *d*-wave superconductor

$$C_d(T)=2\rho_{2D}\begin{cases}9\alpha T^2\zeta(3)/2, & \text{when} \quad \mu>0,\\ \pi^2\beta T/6, & \text{when} \quad \mu\to 0^{\pm},\\ \gamma h(|\mu|,T)\exp-[|\mu|/T], & \text{when} \quad \mu<0.\end{cases} \tag{47}$$

The expression for $\mu<0$ is valid only when $|\mu|\gg T$. Notice the qualitative change in behavior at low temperatures in the vicinity of $\mu=0$. The T^2 behavior for $\mu>0$ is consistent with nodes of the gap function (zeros in the excitation spectrum), and the exponential behavior for $\mu<0$ is consistent with a full gap in the excitation spectrum. The linear temperature dependence at $\mu=0$ arises from the quadratic dispersion found in Sec. IV. The parameter β can be interpreted as measuring the correlations between electrons since it essentially renormalizes the two dimensional electronic density of states ρ_{2D}.

The inclusion of collective modes adds a contribution to the specific heat of the form

$$C_d^{(\rm col)}(T)=-T\frac{\partial^2\Omega_{\rm col}}{\partial^2 T}. \tag{48}$$

In the case of the neutral superconductors (fixed interaction and changing density), the low-energy collective modes have linear dispersion and give a T^2 contribution to the total specific heat in the two-dimensional situation described here for all values of μ. Only the coefficient (prefactor) of the T^2 terms changes as a function μ. Thus, the qualitative changes in the total specific heat are captured by the change in the excitation spectrum of quasiparticles as a function of μ. The same is true in the case of charged superconductors, where the collective mode contributions to the specific heat are exponentially suppressed at low temperatures due to the presence of a gap in the collective mode excitation spectrum for all values of μ.

C. Brief discussion

For completeness, we compare briefly the *s*- and *d*-wave cases. In the *s*-wave case the quasiparticle excitation spectrum is always gapped for all μ (densities) with no qualitative change in the temperature dependence. This leads to an exponential suppression of the quasiparticle contributions to the spin susceptibility and specific heat for all μ (densities). As a consequence the line where $\mu=0$ in the *s*-wave case is not special. In the *d*-wave case, however, gapless quasiparticle excitations become fully gapped when μ becomes negative, thus qualitatively changing the low-temperature thermodynamics of the superconductor. Notice, for instance, that the slopes of C_d and χ_d with respect to temperature are discontinuous at $T=0$ when $\mu=0$, thus indicating the possibility of a quantum phase transition as the density of carriers is reduced below the critical density $n=n_c$ where μ vanishes.

XI. SUMMARY

In summary, using a saddle point approximation, we have studied the low temperature thermodynamic properties in the evolution from BCS to BEC superconductivity for varying density and interaction strength in both *s*-wave and *d*-wave channels. In the *s*-wave case the excitation spectrum is always gapped, and the momentum distribution is a continuous function of μ. However, in the *d*-wave case the excitation spectrum is gapless for $\mu>0$ and acquires a full gap for $\mu<0$. Furthermore, the momentum distribution is discontinuous at low k, as μ crosses zero. As a result, the changes in spectroscopic and thermodynamic properties near $\mu=0$ are dramatic at low temperatures, suggesting the existence of a zero temperature phase transition. In addition, we have noted that the quantum phase transition occurs without a symmetry change and identified it as being topological in nature. Although it is tempting to make a connection to high temperature superconductors, it is not clear that these materials cross the $\mu=0$ ($n=n_c$) line at $T=0$ as the density of carriers n is changed, i.e., the attractive interaction may not be large enough ($\lambda_d<\lambda_{cd}$) in these materials [see Figs. 4(b) and 4(c)]. We can not compare the results of these theoretical considerations to high-temperature superconductors until systematic experimental studies are conducted as a function of density of carriers in the low-temperature superconducting phase, where the evolution from BCS to BEC can be cleanly tested. However, it is theoretically important to continue studying the regime where $\mu\simeq 0$, as the line of $\mu=0$ ($n=n_c$) in the n versus λ_d plane seems to correspond to a quantum critical line separating a gapless *d*-wave superconductor ($\mu>0$) from a fully gapped *d*-wave superconductor ($\mu<0$), as supported from the preliminary calculations of compressibility, specific heat, and spin susceptibility.[21]

ACKNOWLEDGMENTS

We would like to thank the Georgia Institute of Technology, NSF (Grant No. DMR-9803111), and NATO (Grant No. CRG-972261) for financial support. In addition, one of us (C. A. R. S. de M.) would like to thank the Aspen Center for Physics, and Professor Peter Littlewood (Cambridge University) for their hospitality.

[1] D.M. Eagles, Phys. Rev. **186**, 456 (1969).

[2] A.J. Leggett, in *Modern Trends in the Theory of Condensed Matter*, edited by A. Pekalski and J. Przystawa (Springer-Verlag, Berlin, 1980); J. Phys. Colloq. **41**, C7-19 (1980).

[3] P. Nozières and S. Schmitt-Rink, J. Low Temp. Phys. **59**, 195 (1985).

[4] R. Micnas, J. Ranninger, and S. Robaszkiewicz, Rev. Mod. Phys. **62**, 113 (1990).

[5] M. Randeria, J.M. Duan, and L.Y. Shien, Phys. Rev. B **41**, 327 (1990).

[6] M. Drechsler and W. Zwerger, Ann. Phys. (Leipzig) **1**, 15 (1992).

[7] S. Stintzing and W. Zwerger, Phys. Rev. B **56**, 9004 (1997).

[8] F. Pistolesi and G.C. Strinati, Phys. Rev. B **53**, 15 168 (1996).

[9] B. Janko, J. Maly, and K. Levin, Phys. Rev. B **56**, R11 407 (1997).

[10] S.K. Adhikari and A. Ghosh, Phys. Rev. B **55**, 1110 (1997).

[11] C.A.R. Sá de Melo, M. Randeria, and J.R. Engelbrecht, Phys. Rev. Lett. **71**, 3202 (1993).

[12] J.R. Engelbrecht, M. Randeria, and C.A.R. Sá de Melo, Phys. Rev. B **55**, 15 153 (1997).

[13] V.P. Gusynin, V.M. Loktev, R.M. Quick, and S.G. Sharapov, Int. J. Mod. Phys. B **12**, 3035 (1998).

[14] L.S. Borkowski and C.A.R. Sá de Melo, cond-mat/9810370 (unpublished).

[15] B.C. den Hertog, Phys. Rev. B **60**, 559 (1999).

[16] N. Andrenacci, A. Perali, P. Pieri, and G.C. Strinati, Phys. Rev. B **60**, 12 410 (1999).

[17] Quite generally any short ranged real space potential $V(r)$ with range R_0 leads to a $V^{(l)}_{kk'}$ which is separable for small momenta, provided that $kR_0\ll 1$ *or* $k'R_0\ll 1$. In the simpler limit when both $kR_0\ll 1$ *and* $k'R_0\ll 1$, $V^{(l)}_{kk'}\simeq k^l k'^l(2\pi/2^{2l})\int_0^\infty dr\, r^{2l+1}V(r)$, where l is assumed to be positive for definiteness. Notice here that $V^{(l)}_{kk'}\propto k^l k'^l$, thus for the *s*-wave case $V^{(s)}_{kk'}\propto$ const, while for the *d*-wave case $V^{(d)}_{kk'}\propto k^2k'^2$. In the opposite limit, $kR_0\gg 1$ *or* $k'R_0\gg 1$, the potential $V^{(l)}_{kk'}$ is certainly not separable. In the simpler limit when both $kR_0\gg 1$ *and* $k'R_0\gg 1$, $V^{(l)}_{kk'}$ mixes different $\mathbf{k}$ and $\mathbf{k}'$ and shows an oscillatory behavior which is dependent on the exact form of $V(r)$, with a decaying envelope proportional to $k^{-1/2}k'^{-1/2}$.

[18] Appropriate choices of λ_d, k_0, and k_1 in the potential $V^{(2)}_{k,k'}$ ($l=2$) lead to a lower ground state energy W_2 as a function of density (even at low densities) in comparison with the *s*-wave ground state energy W_0 controlled by λ_s and k_0. However, the respective interaction parameters in *s*-wave and *d*-wave are treated independently, because we make the underlying assumption that different mechanisms cause pairing in these channels.

[19] One can safely neglect residual interaction when $k_F^2\ll k_0^2$ and pairing between $(-\mathbf{k},\mathbf{k})$ states is sufficient to describe the BCS to BEC evolution. However, when $k_F^2\gg k_0^2$, residual interactions become important and pairing between $(-\mathbf{k},\mathbf{k})$ states is no longer sufficient.

[20] G.E. Volovik, *Exotic Properties of Superfluid ^3He* (World Scientific, Singapore, 1992).

[21] We are currently taking fluctuations into account through residual quasiparticle interactions and finite temperature effects, as well as performing a renormalization group study in two and higher spatial dimensions, which will allow us to construct a more accurate phase diagram at low temperatures and a renormalization flow chart.

[22] P.M. Chaikin and T.C. Lubensky, *Principles of Condensed Matter Physics* (Cambridge University Press, Cambridge, 1995).

[23] N.D. Mermin and H. Wagner, Phys. Rev. Lett. **17**, 1133 (1966).

[24] N.D. Mermin, Phys. Rev. **176**, 250 (1968); Phys. Rev. B **20**, 4762(E) (1979).

[25] V.L. Berezinskii, Zh. Eksp. Teor. Fiz. **59**, 907 (1970) [Sov. Phys. JETP **32**, 493 (1971)]; **61**, 1144 (1971) [**34**, 610 (1972)].

[26] The effects of quantum and thermal fluctuations on this topological phase transition remain to be investigated in two and higher dimensions. See Ref. 21.

[27] I.M. Lifshitz, Zh. Eksp. Teor. Fiz. **38**, 1569 (1960) [Sov. Phys. JETP **11**, 1130 (1960)].